Emerging Trends in Ultrasound Imaging

Chapter 1

Transmission Ultrasound Imaging Using 3D Inverse Scattering

John C Klock[1*]; Mark W Lenox[1]; James W Wiskin[1]; Bilal Malik[1]; Rajni Natesan[1]

[1]QT Ultrasound Labs, Novato, California

*[*]**Correspondence to: John C Klock,** QT Ultrasound Labs, 3 Hamilton Landing Suite 160, Novato CA 94949*

Email: john.klock@qtultrasound.com

1. Definition

Transmission ultrasound is the method by which a pulse pressure-wave of sound is propagated through an object and transmitted sound energy is measured at a number of receivers on the opposite side of the object. This differs from standard reflection or B-Mode ultrasound which uses a single transducer to both transmit and measure the signal reflected back toward the original source. By propagating the wave through the object, the full effects of refraction, diffraction, and attenuation are applied to the wave and that information is now available at the receiver. This information can be recovered by using the Helmholtz wave equation in a technique called inverse scattering. There are a variety of ways to solve the Helmholtz equation, going from simple straight-ray techniques to more sophisticated full-wave 3D non-linear methods.

Keywords: 3D ultrasound; Transmission ultrasound; Inverse scattering; Ultrasound tomography; Breast imaging

2. History

Real-time, reflection-based hand held ultrasound (HHUS), better known as the fast B-scanner, was developed by Walter Krause, Richard Soldner, Johannes Paetzold and Otto Kresse and manufactured as the Vidoson® by Siemens Medical Systems of Germany in 1965 [1]. HHUS has been used as a primary adjunctive modality for diagnostic imaging, including biopsy guidance; however, there are several acknowledged issues with HHUS. These include limited tissue identification, operator and reader variability, and a small field of view and range when high-resolution transducers are used. Also, results can be difficult to reproduce, as it is operator dependent and not quantitative in nature. Nevertheless, it has been shown to

be valuable in many different areas of medicine. In breast imaging, for example, it has been useful in screening dense breasts and determining solid from cystic masses. Creating a 3D volumetric image of the breast and its tissue characteristics with ultrasound has been a notable goal for the past several decades, but it has not been achieved until recently by images created using transmission ultrasound.

3. Challenges of Transmission Ultrasound

To create *ab initio* accurate breast ultrasound images in 3D, one must pulse sound energy through the tissue and measure the resulting sound energy on the opposite side of the object using a detector array. The mathematical solution to generate images from the raw ultrasound data involves solving the Helmholtz wave equation. This equation governs how acoustic waves propagate through a medium. Helmholtz is a complex partial differential equation and there are many ways to solve it that vary in their own complexity. Kaveh et al. [2] in 1980 first applied the Born approximation to the inverse problem (an approximate solution/ inversion of the Helmholtz equation). This is needed to predict and observe the diffraction of the sound as it passes through tissue. Linear solutions like the Born approximation are simpler and computationally less demanding but result in poor image quality. Full wave, non-linear solutions like Lippmann-Schwinger are more complex, produce better images, and are considered the gold standard. Although there are image quality advantages to the Lippmann-Schwinger solution, there are several distinct problems with it as well. The full solution considers multiple scattering, diffraction, refraction and attenuation. Unfortunately, this makes the solution numerically difficult and time consuming. Various approximations have been employed over the years to make the computation easier, but they degrade the quality of the image in various ways.

The basic straight-ray method was discovered by Radon in 1917 [3]. The modern era of transmission ultrasound imaging began with the pioneering work of Greenleaf et.al, in 1974 where straight-ray tomography was originally used. Although the resulting images were crude by today's standards, they showed that quantitative information could be obtained [4,5]. Following that work, Johnson used a non-linear method to invert the Helmholtz equation that was the first instance of a true full wave non-linear solution to the imaging problem [6-8]. In the 1980's, Johnson et al. showed that a non-linear solution of the full wave equation was possible and desirable, but computationally very expensive. With the advent of extremely powerful computers at very low cost, this has become the current state-of-the-art.

Others have created 2D images of the breast in the coronal direction, in a similar fashion to a breast tomogram [9-13]. The first instance of a transmission image in vivo was Glover [15]. However, in this chapter, we concentrate on the water bath scanner being developed presently by QT Ultrasound Labs, Inc., and discussed in [14,17]. Some water bath scanners

utilize straight and bent ray-based techniques, which do not fully incorporate diffraction effects, but the QT system utilizes 3D model-based non-linear inverse scattering techniques developed by Johnson for the transmission mode images. To make the method computationally practical, full 3D inverse scattering transmission ultra sound uses a parabolic (paraxial) approximation to the full Helmholtz equation. This is a relatively simple approximation to Lippman-Schwinger and in practice; the paraxial method has been shown to produce very good image quality in a reasonable period of time.

4. A Practical Full 3D Transmission Ultrasound Imaging System

While transmission ultrasound has been investigated as an adjunct to mammography for quite some time [15,16], recent developments in hardware and imaging algorithms have enabled very marked improvements in spatial resolution and clinical utility. A clinical transmission ultrasound 3D inverse scattering imaging system uses a transmitter – receiver array pair as well as a system of reflection transceivers to create a multi-modality system (transmission and reflection). Physically, a transmitter and receiver pair are co-located with multiple transducers of various focal lengths in a U-shaped arrangement as shown in Figure 1. In transmission mode, the transmitter emits a plane wave that is received by the receiver. In reflection mode, the reflection transducers send and receive their own information at each position. Multiple transmission acquisitions are acquired for 180 angles as the U-channel is rotated fully around the subject. Reflection data is acquired from the reflection transducers and it is interleaved between the transmission acquisitions. Once acquired, the transmission projection information is reconstructed using nonlinear inverse scattering in 3D. The result of the reconstruction is a 3D image volume of speed-of-sound (SOS) and attenuation-of-sound (AOS). The SOS image is useful diagnostically by itself and this will be discussed in later sections. The reflection information is compounded together after being refraction corrected using the SOS image. Without refraction correction, the reflection information is imprecise and not as useful clinically. With refraction correction, contrast resolution under 100µm is commonly achieved in compounded B-Mode reflection images. An example SOS image is shown in **Figure 2**.

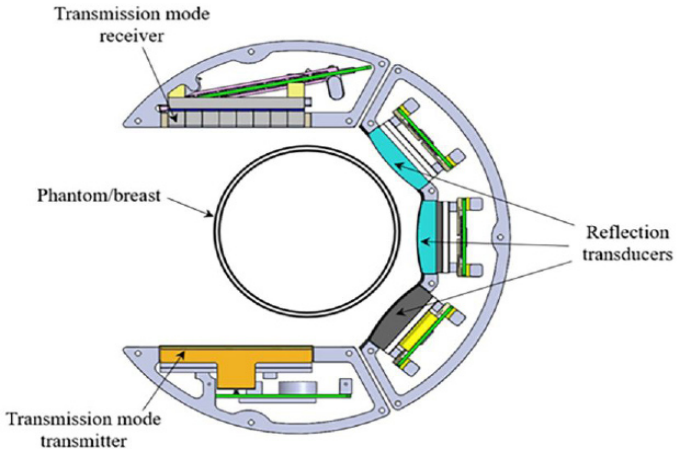

Figure 1: System Geometry of the QT Ultrasound® full 3D transmission ultrasound imaging armature with the plane-wave transmitter, receiver and the reflection transducers, all of which rotate 360 degrees around the part to be imaged.

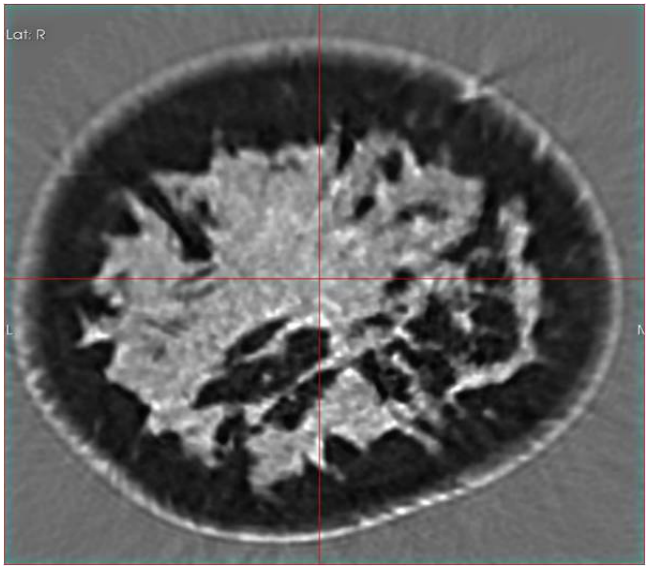

Figure 2: Example of a Speed-of-Sound image using full 3D transmission ultrasound imaging.

5. 2D versus Full 3D Transmission Imaging

Nearly all medical imaging technologies acquire data on a single plane (2D) and use some sort of filtered back-projection algorithm to generate 2D slices for clinical interpretation. This works because typical energy types used for medical imaging (X-rays, or gamma rays) can be modeled using the Radon transform. Ultrasound energy does not conform to the Radon transform and must be modeled using the wave equation. The QT Ultrasound® technology uses a full 3D inverse scattering algorithm. The difference between 2D and 3D image acquisition is illustrated in **Figure 3**.

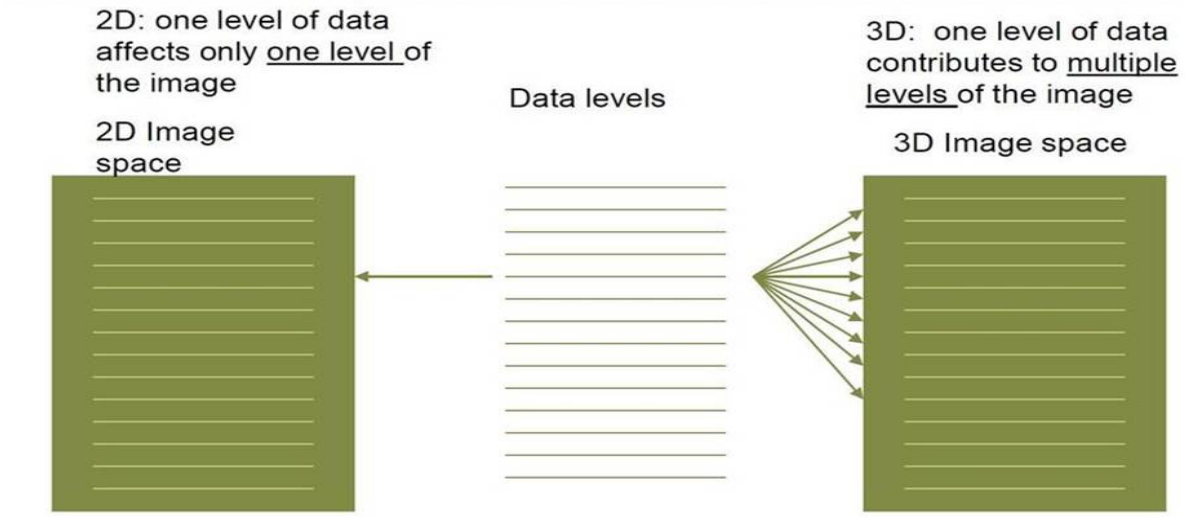

Figure 3: Schematic of information flow for 2D versus 3D Image Acquisition.

In imaging modalities based on the radon transform (CT, PET, SPECT, etc.), loss in imaging performance due to the 2D nature of the data acquisition is relatively limited because the fraction of events that are scattered are relatively small, normally under 30% in the worst case. In this case, scattered information is simply noise because the radon transform is a line integral and anything that falls off that line is thrown away. This does not hold for ultrasound-based modalities because the wave propagation is based on the Helmholtz wave equation which

is a 3D model. As the wave propagates through the volume, where it is bent due to refraction, diffraction or attenuation, this information is carried forward with the wave until it reaches the receiver. In this way, transmission ultrasound is fundamentally different than all other modalities in that these effects are not considered noise, they are the signals to be recovered in the reconstruction. These effects occur not just in the 2D plane, but occur in all directions, so it is fundamentally required to acquire the raw data in 3D in order to fully recover the signal. Attempts to recover the information in 2D only are fundamentally restricted in available image quality. This full 3D image acquisition paired with a full 3D reconstruction method provides images of high fidelity with dramatically reduced artifacts [17,18] as shown in **Figures 4** and **Figure 5**.

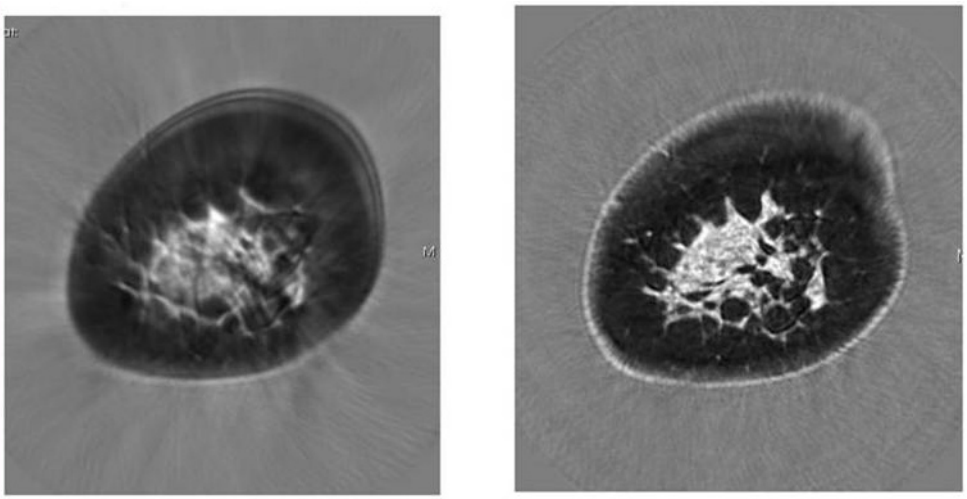

Figure 4: Coronal images of the same breast reconstructed from 2D versus 3D.

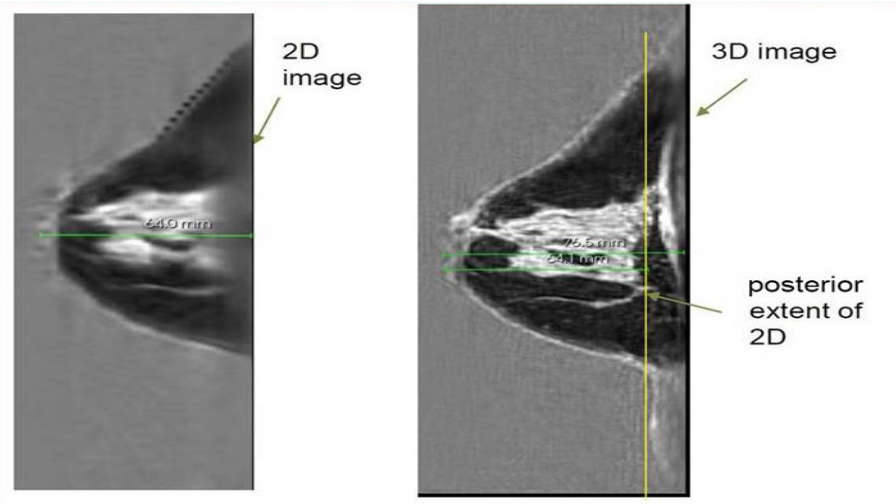

Figure 5: Sagittal images of the same breast reconstructed from 2D versus 3D.

Multi-modality systems like the QTultrasound™ device perform both transmission and reflection in the same system. In reflection mode, each of the three reflection transducers with different focal lengths are fired independently in a B-mode acquisition for each angle, and the resulting images are compounded together and corrected for refraction using the speed map computed in the transmission phase. This compounding produces a non-quantitative image that is proportional to impedance mismatch, referred to simply as reflection units. Since impedance mismatch for ultrasound waves indicates a change in tissue type, these images have high

resolution, and highlight edges of tissue. This phenomenon is very instructive of anatomical reference. Due to the nature of this type of compounding, speckle is dramatically reduced, but the resulting image can be read very much like a traditional B-Mode image.

Normal B-Mode reflection ultrasound suffers from the effects of refraction as the beam propagates through the object being scanned. Refraction is governed by Snell's Law which states that the change in angle of an incident wave to a boundary is proportional to the ratio of the velocities of the wave in the two media. Normally, these effects are simply ignored because there is no way to correct for them as normal B-Mode ultrasound devices do not have the ability to measure the speed of sound within a given object. In this way, the multi-modality nature of a typical transmission ultrasound system is very complimentary, and the SOS map generated with transmission can be used to correct the reflection images for refraction. This correction puts every voxel in the reflection images in the correct location in 3D space. When all the reflection images are assembled through the compounding process, they all line up correctly and structures within the imaging volume appear as they should. Examples of the effects of refraction correction are shown in **Figure 6**.

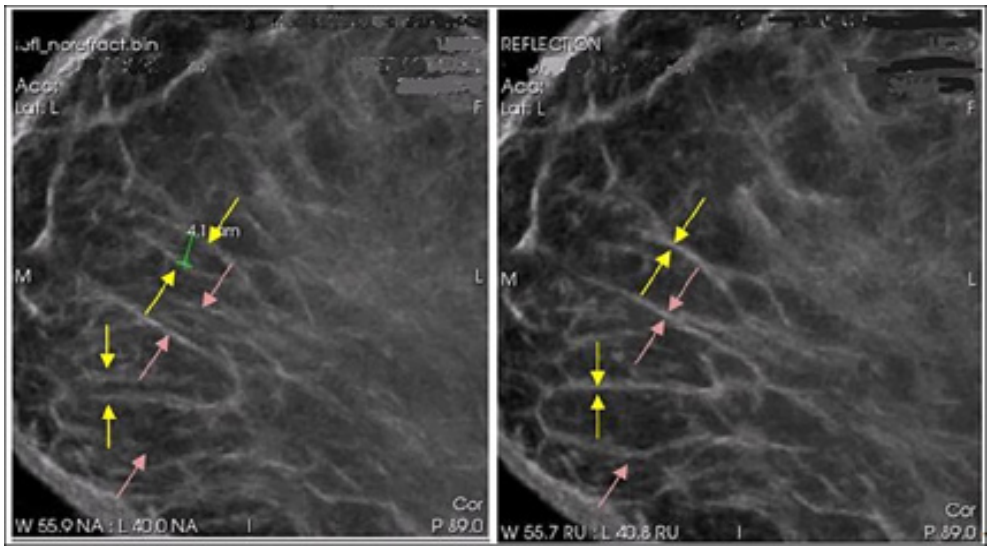

Figure 6: Reconstruction of the reflection image using data uncorrected (left) and corrected data (right).

The result of each scan is a stack of slices of two different types, Speed and Reflection. These image stacks are precisely co-registered since they were acquired at the same time and can be put together to form a 3D view of the object in the field-of-view (FOV). The 3D nature of the device allows the evaluation of both 2D qualities, like dimension and relative placement, as well as 3D physical qualities, such as the volume of a structure and the quantitative evaluation of the speed-of-sound within the entirety of that volume.

6. Phantom Studies to Predict Clinical Performance

One of the strengths of modern ultrasound methods is that it has very high contrast. The higher the contrast, the easier it is to see small isolated structures and to separate adjacent structures. This is at odds with the typical performance we see with imaging modalities that

have much less contrast such as CT. Those modalities require much higher intrinsic resolution to achieve the same perceived image quality. By using inverse scattering in transmission ultrasound, we achieve both high resolution and high contrast simultaneously and this makes it possible to clinically perceive objects that are very small. The real question is how small this can occur reliably. In Figure 7, we show a nautilus phantom where the size of the targets gets progressively smaller, all the way down to 400 microns with very little blurring.

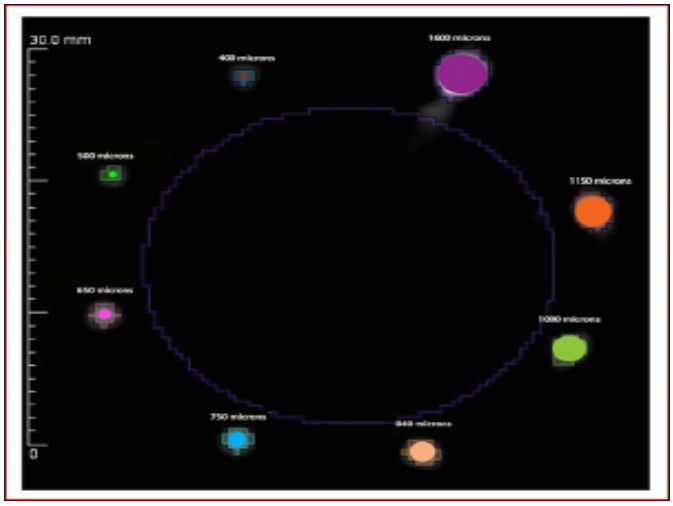

Figure 7: Nautilus phantom showing high speed targets varying from 1600-400 microns.

challenge in understanding what a clinician should be able to clinically identify using high resolution ultrasound is a complex problem because both resolution and contrast come into play. The first step in understanding and thus predicting the potential clinical performance is to measure the performance of the system in two ways. First, we need to understand how well it can physically measure the size of an object. This is sometimes referred to as the intrinsic resolution and it is measured with a standard called the point spread function (PSF). Second, we need to determine how well the system can discern between different types of material. We refer to this measurement as contrast and it is measured by looking at the contrast to noise ratio (CNR) for various size objects. In the following sections we will discuss how these are measured and how a high-resolution 3D ultrasound system performs using those measures.

A. Point Spread Function

There are no types of cameras able to exactly take an image of an object all the way down to the atomic level and accurately reproduce that. All cameras take an image that is a sampled or blurred version of the actual reality. In the same way that a 10-mega pixel photographic camera takes a sharper picture than a 1 mega pixel camera, the number of pixels in a camera is directly related to the PSF. Cameras with more resolution or more pixels have a smaller PSF and generally take a sharper image. In medical imaging we use PSF rather than mega pixels because it is a very precise way of determining the true performance. The point spread function (PSF) is the magnitude of the inherent blur produced by the system. In a way, the PSF is related to the smallest size object that can be accurately measured. Objects smaller than the

PSF will be blurred out. The PSF represents the uncertainty of using the device to perform spatial measurements and in many ways the clarity of the resulting image.

The PSF can be measured by placing an object in the field of view of a known size and measuring the size of the object with the system. Due to imperfections in the measurement, uncertainty, blur, and sampling, the measured size will be slightly larger than the actual size. The difference in size of what is measured and the actual size is related to the PSF. Since we assume noise to be Gaussian in nature, we can simply deconvolve the measured size (m_{obj}) from the actual size (m_{actual}) using the sum of squares method to determine the blurring component.

$$PSF = \sqrt{{m_{obj}}^2 - {m_{actual}}^2}$$

An example line plot across a very small object (in a reflection image) and plot are shown in Figure 8. The PSF is simply the full width at half maximum (FWHM) of the peak in the line plot because the actual size of the object is very small. The resulting PSF for speed of sound (SOS) in all directions is shown in **Table 1** and the same for reflection in **Table 2**.

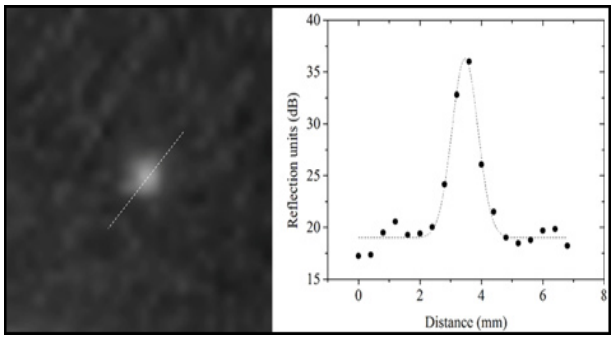

Figure 8: Reflection image of a 100µm point scatterer and the resulting line profile used to determine the PSF**.**

Table 1: Speed of Sound point spread function.

Position	*FWHM (mm)*
X and Y	1.49 ± 0.07
Z	2.35 ± 0.11

Table 2: Reflection point spread function.

Position	*FWHM (mm)*
X and Y	0.98 ± 0.07
Z	2.59 ± 0.09

B. Contrast-to-Noise

In addition to resolution, the detectability of an object also involves determining how strong a signal is in relation to the background noise and is referred to as Contrast-to-Noise ratio (CNR). The larger the CNR of an object, the more visible the object is relative to the background. Transmission ultrasound provides very high CNR for small targets because the ultrasound wave interacts with everything it touches, and this information is carried forward into the image after it is reconstructed.

The contrast to noise measurement of any given modality is the ratio of the signal over a background divided by the standard deviation of the background. This is a measure

of sensitivity in that it determines how well the observer should be able to detect a structure against background noise. It is measured by selecting a region of interest (ROI) that is the actual size of the object and measuring the signal S_{obj} of the object as well as a larger background ROI where we measure the background signal S_{bkd} and the standard deviation of the background δbkd. These values are then applied in the following way to compute CNR:

$$CNR = \frac{S_{obj} - S_{bkd}}{\delta_{bkd}}$$

For SOS measurements, we fabricate a phantom made of polyurethane with embedded polyurethane rods of known speed and size. The sizes of the rods are 20, 10, 5, and 1.4mm in diameter. This resulted in the CNR values in **Table 3**.

Table 3: Contrast-to-noise values for speed of sound imaging.

Object size (mm)	Mean ROI Speed (m/s)	Speed of sound CNR mean ± s.d.	Speed of sound CNR mean ± s.d. (dB)
20	1531.6	54.9 ± 0.70	17.4 ± 0.06
10	1527.2	53.8 ± 1.20	17.3 ± 0.10
5	1529.3	55.2 ± 0.58	17.4 ± 0.04
1.4	1497.5	36.9 ± 2.17	15.6 ± 0.26

For Reflection measurements, we fabricate a phantom made of Agar and imbedded soda lime glass bead reflectors (Cospheric, LLC) in sizes ranging from 1mm to 0.1mm. CNR measurements for reflection data are shown in **Table 4**.

Table 4: Contrast-to-noise values for reflection imaging.

Object size (mm)	Mean ROI intensity (RU)	Reflection CNR mean ± s.d.	Reflection CNR mean ± s.d. (dB)
1	3738919	11078.3 ± 2038.1	40.4 ± 0.8
0.8	2808618	8292.5 ± 735.5	39.2 ± 0.4
0.55	2735874	7972.4 ± 755.9	39.0 ± 0.4
0.3	2526247	7447.5 ± 1452.1	38.7 ± 0.9
0.2	2025683	5682.2 ± 562.1	37.5 ± 0.5
0.1	519652	1377.3 ± 137.4	31.3 ± 0.4

These studies have been reported in [19, 20].

C. Summary of Performance: Contrast Resolution

Since both contrast and resolution have an effect on detection ability and thus clinical effectiveness, a combined measure is required to quantify this effect. This measure is Contrast Resolution (CR), sometimes referred to as Clinically Effective Resolution. It is the size of the smallest object that can be reasonably detected in clinical practice. Contrast Resolution is an adjunct to the CNR and it is defined as the smallest object of a type you wish to detect that

still maintains a minimum 10:1 CNR against a normal background. In this way, it brings both resolution (the size of the target object) and the ability to see the object (contrast) into a single measure.

When CNR is measured, simply measuring a variety of size targets allows us to simply select the smallest target with a CNR at least 10:1. In the case of high resolution ultrasound, it is very difficult to get small enough to go past the 10:1 limit. From the results in Table 3, the smallest object measured is 1.4mm with a CNR of 15.6 dB. This suggests that the maximum Contrast Resolution for speed of sound imaging is less than 1.4mm. From the results in Table 4, the smallest object measured is 100μm with a CNR of 23.1. This suggests that the maximum Contrast Resolution for reflection imaging is less than 100μm.

In the case of speed-of-sound imaging, we can expect visibility of an object smaller than 1.4mm in clinical conditions with a margin for error. For reference, this is less than half the diameter of a BB and substantially smaller than the effective clinical limits of mammography for solid lesion detection. In a study by Nickson in 2009 of over 1000 cancers detected, mean tumor size for first diagnosis was 13mm for women of all body types [21] using mammography. This is almost an order of magnitude larger than full-wave 3D transmission ultrasound. In the case of reflection imaging, we can expect visibility of hard targets like micro-calcifications down below 100 microns. For reference, this is roughly the size of a single human fat cell. This is very good performance for an *in vivo* imaging system.

7. Clinical Studies of a Full 3D Transmission Ultrasound Imaging System

Clinical studies require a device that has been developed regarding safety for human subjects and performed under the approval of an Institutional Review Board (IRB). The device shown in Figure 9 is the QT Ultrasound breast scanning system which was FDA cleared as an adjunct to mammography in 2017. This system has both 3D acquisition as well as 3D reconstruction and is fully quantitative, thus the name Quantitative Transmission Ultrasound.

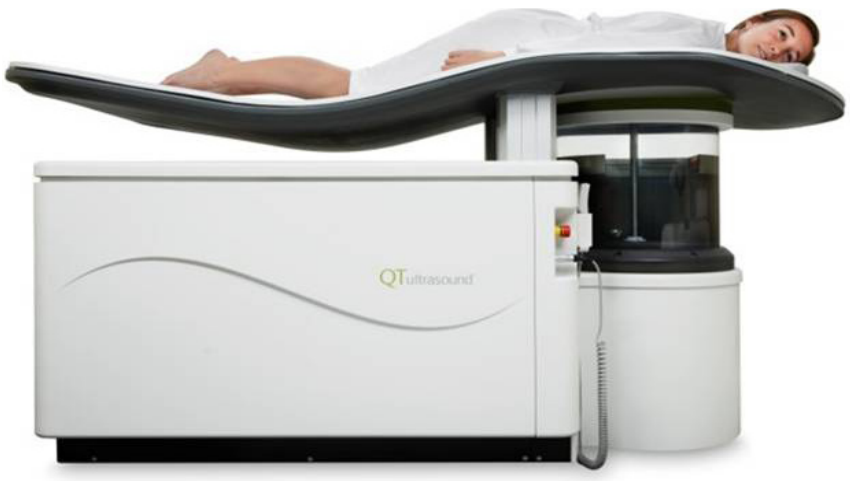

Figure 9: Transmission ultrasound system currently being commercially developed by QT Ultrasound Labs, Inc.

The 3D volume acquisition has the following features for imaging of the breast: 1) quantitative accuracy throughout the imaging volume, 2) image quality is uniformly high, 3) ability to image the entire breast from nipple to the pectoralis in a single scan–hence the retromammary fat interface becomes visible. Furthermore, segmentation of skin, fat, connective, ducts, glands, cysts, fibroadenomas and cancers can be done effectively due to a high degree of quantitative accuracy made possible by acquiring and reconstructing the images in 3D.

A. Microanatomy

It has been shown that transmission ultrasound can be used to evaluate the pathology of breast lesions in a variety of clinical situations. The ability to perform this evaluation is largely due to both the fact that the speed of sound is directly related to the bulk modulus of the material and the structural changes to the tissues that arise from various pathologies that affect the bulk modulus. This relationship suggests that direct speed-of-sound measurements have positive potential to discriminate various pathologies, including those that exhibit some type of calcification. Full 3D transmission ultrasound provides a stable measure of both geometry and speed-of-sound on objects as small as 0.4mm in diameter, and possibly smaller. Clinical trials have been done using receiver-operating-characteristic analysis of a QT Ultrasound® system in evaluating all breast structures including microcalcifications [22-27]. The technology has been used in a variety of clinical settings and the images are unique to the methods used [22] as seen in **Figures 10 and 11**.

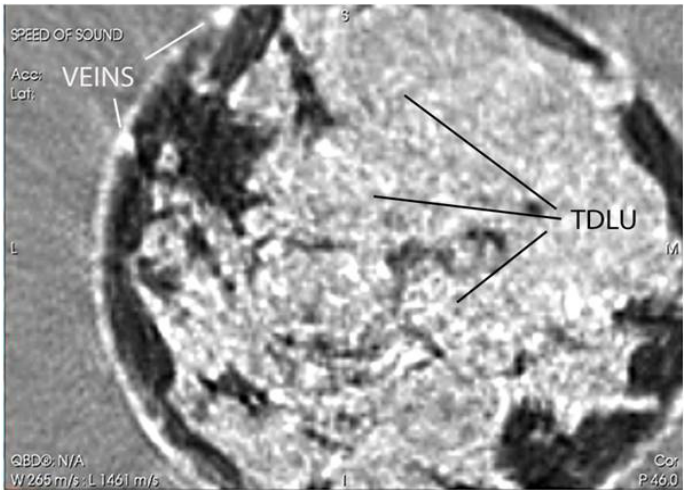

Figure 10: Transmission ultrasound image (coronal view) showing "speckled" glandular tissue and the terminal ductal lobular units (TDLU) of the breast.

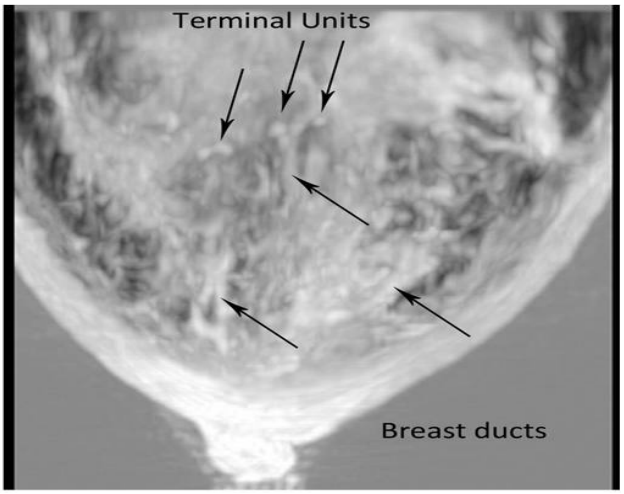

Figure 11: Transmission ultrasound image (axial view) showing ductal and glandular tissue and the terminal ductal lobular units (TDLU) of the breast.

B. Biomarkers

Because the transmission mode of the scanner gives a quantitative speed of sound value for each voxel within the 3D breast dataset, there is the potential for that speed of sound value to be used as a discriminator of breast tissue type [22] as shown in **Figure 12**. In the

published studies of full 3D transmission ultrasound imaging, it was shown that the technology can perform breast tissue image classification. It was demonstrated that it was possible to differentiate features of all the normal breast tissue types [23] including skin, fat, glands, ducts or connective tissue with an overall accuracy of greater than 90%. Finally, the classifier was validated on whole breast image volumes to provide a color-coded breast tissue volume. This is shown in **Figure 13**.

Breast tissue speeds
(Mean ± SD)

Speed (M/S)	1400	1425	1450	1475	1500	1525	1550	1575	1600	1625
Skin (1529–1537)										
Cooper ligaments (1422–1496)										
Ductal tissue (1560–1612)										
Glandular tissue (1517–1567)										
Fat (1418–1436)										

Figure 12: Summary analysis of 250 tissue measurements of speed of sound taken from 3 cadavers and 4 normal volunteers. Bars represent mean and 1 SD.

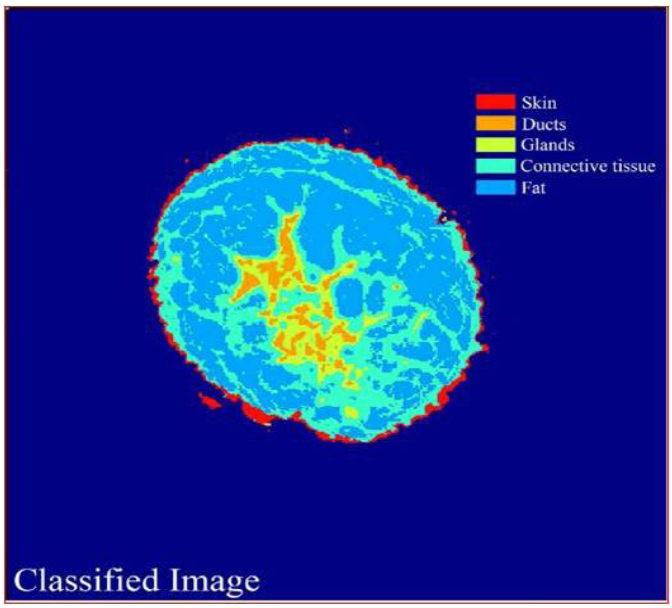

Figure 13: Image classification using the SVM classifier. The speed of sound, attenuation and reflection images are used together by the classifier to generate a respective tissue-color-coded classified image.

This type of classification has been used in clinical breast imaging to discriminate fine anatomic features, the validation of tissue "biomarkers" and for discriminating normal from abnormal tissues. As an example, this classification system has been used to classify cystic versus solid lesions [24]. Using the readers' binary classification of cyst or solid lesions, the mean sensitivity and specificity were 0.933 [95% CI: 0.837, 0.995] and 0.858 [95% CI: 0.701, 0.985], respectively. When the readers' confidence scores were used to distinguish a cyst versus solid, the mean receiver operating characteristic area was 0.920 [95% CI: 0.827, 0.985]. This is shown in **Figure 14**.

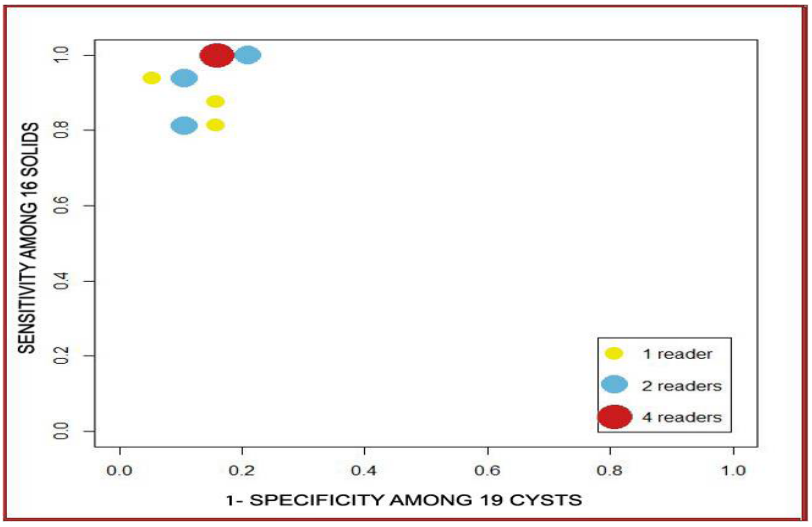

Figure 14: Estimated sensitivity and false positive results among 13 readers for transmission ultrasound.

C. Visual Grading Analysis

To compare the image quality of full 3D transmission ultrasound with digital mammography and hand-held ultrasound, multiple readers scored the image quality of transmission ultrasound compared to the other two modalities using an ordinal rating scale. The proportion of breasts where the image quality was rated better on transmission ultrasound was reported for each feature including different ACR BI-RADS® breast density classes. Using x-ray mammography as a comparator, readers scored transmission ultrasound images as equivalent or better in more than 90% of breasts. Using hand-held ultrasound as a comparator, readers scored transmission ultrasound images as equivalent or better in more than 80% of breasts. In the analysis by breast density, there was no significant change in the performance by transmission ultrasound for any density subtype [23,25]. This is shown in **Figures 15 and 16.**

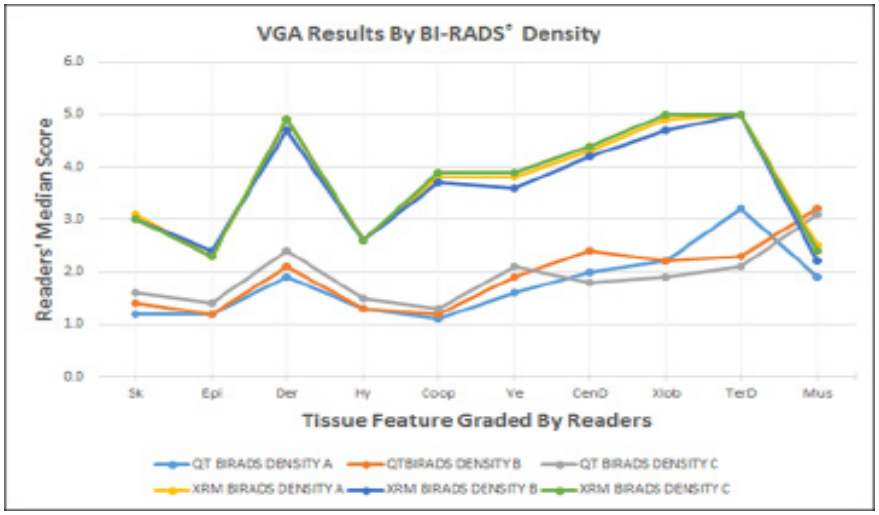

Figure 15: Readers' median image quality score by modality (x-ray mammography vs QT Ultrasound), BI-RADS® density and breast feature: skin (overall), epidermis, dermis, hypodermis, Cooper's ligaments, superficial veins, central ducts entering nipple, intermediate or peripheral ducts (extra-lobular ducts), terminal ductal lobular units, and pectoralis muscle (chest wall). A higher score indicates LESS visibility

These studies confirm that transmission ultrasound can adequately see all the major anatomical features of the human breast that can be seen by no other routinely used clinical

imaging method, including accurately visualizing ductal and glandular tissue detail, even in dense breasts.

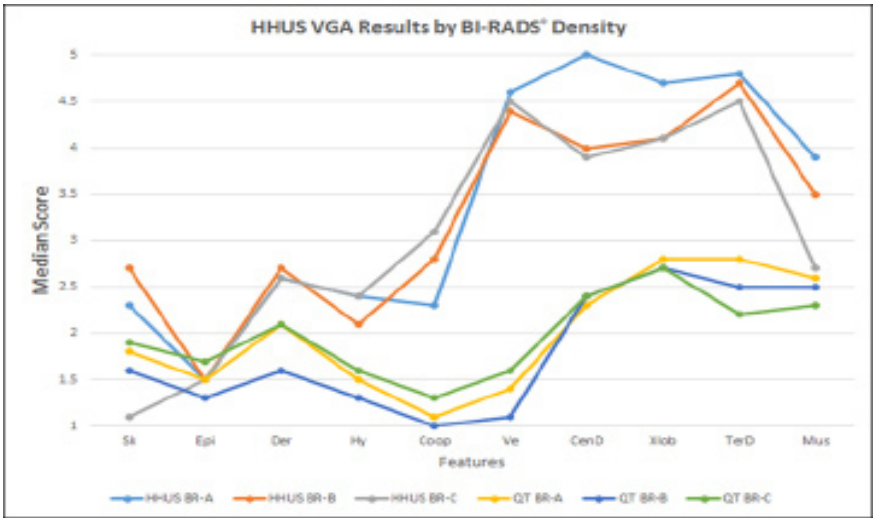

Figure 16: Readers' median image quality score by modality (hand-held ultrasound vs QT Ultrasound), BI-RADS® density and breast feature: skin (overall), epidermis, dermis, hypodermis, Cooper's ligaments, superficial veins, central ducts entering nipple, intermediate or peripheral ducts (extra-lobular ducts), terminal ductal lobular units, and pectoralis muscle (chest wall). A higher score indicates LESS visibility.

D. Breast Microcalcification Detection

Detection of microcalcifications plays an important role in early breast cancer diagnosis. This is demonstrated by a significant number of non-palpable breast cancers that are detected on mammography by examining only the morphology and distribution of microcalcifications. While conventional handheld ultrasound (HHUS) has been a mainstay of diagnostic breast imaging, the ability of conventional HHUS for evaluation of breast microcalcification is somewhat limited and the results to date do not support the clinical use of HHUS for this application. Some of the limitations of HHUS are addressed by Quantitative Transmission ultrasound which is a relatively new imaging paradigm and has shown significant promise in breast imaging. Full 3D inverse scattering transmission ultrasound has been applied to detection of microcalcification. Specifically, it has been shown [26] that QT reflection imaging can detect microcalcification of size up to an order of magnitude smaller than the intrinsic resolution of the system. Imaging in custom fabricated phantoms show that the ability of QT imaging to detect calcium, as measured by contrast to noise ratio, is superior to mammography. Breast imaging performed in cadaveric tissue and in clinic demonstrates the strength of QT towards detection of microcalcification. **Figures 17** through 19 demonstrate how this is performed.

These studies show that: 1) QT reflection imaging is highly sensitive for the detection of microcalcification, 2) QT images demonstrate slightly higher contrast-to-noise ratio in comparison to XRM, and 3) although sub-millimeter calcifications are not visible on the transmission ultrasound image, the, speed-map based refraction correction aids in visualization of microcalcifications in reflection ultrasound images.

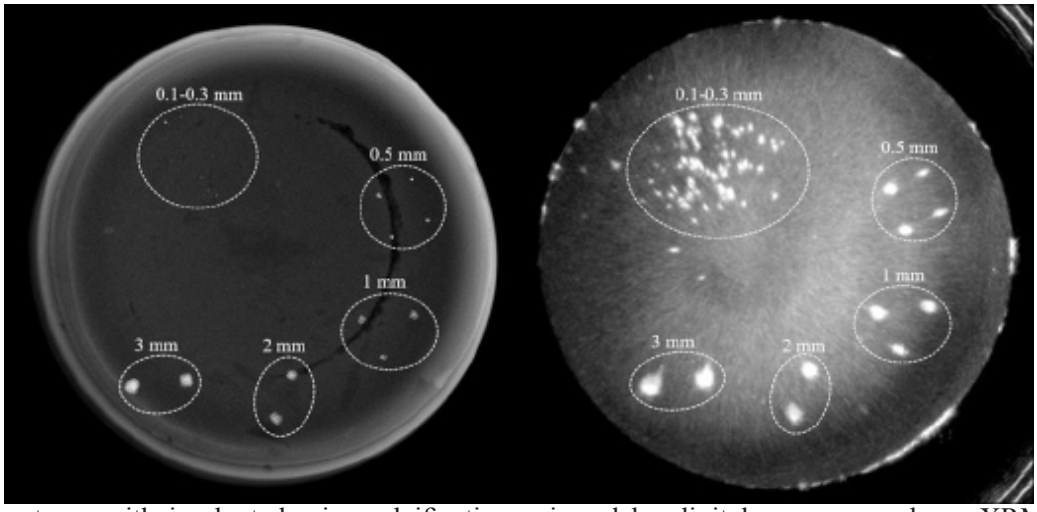

Figure 17: Phantoms with implanted microcalcifications viewed by digital mammography – XRM (left) and QT ultrasound (right). Note that for particles >500µm, QT reflection images exhibit 23% higher CNR than XRM; for particles <500µm, QT reflection images exhibit 76% higher CNR than XRM.

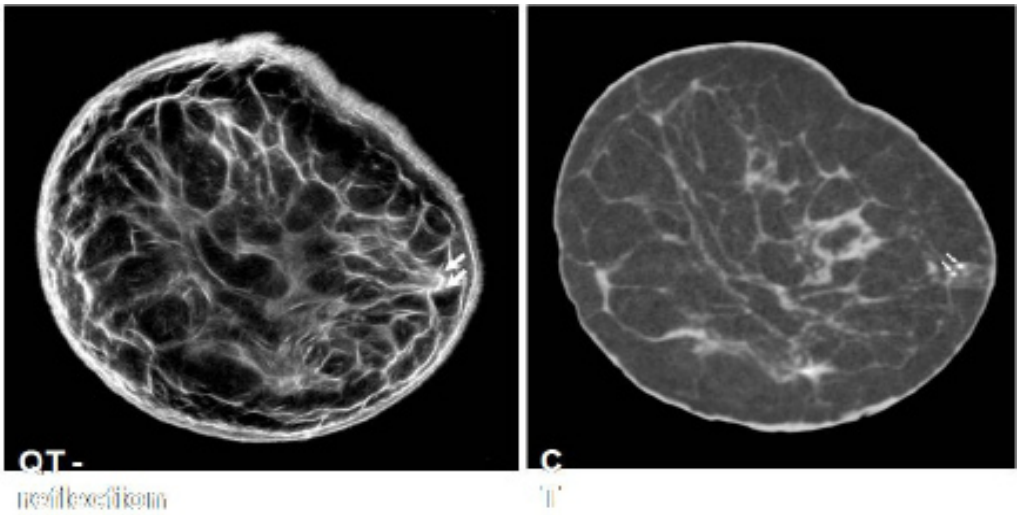

Figure 18: Visualization of microcalcifications in a cadaver breast.
The left image shows the QT scan and the right image shows the CT scan.

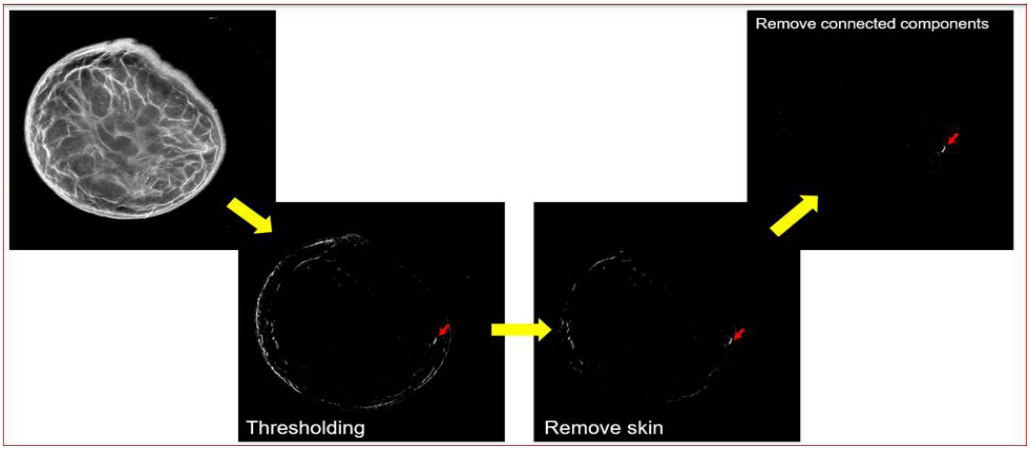

Figure 19: This figure demonstrates how thresholding and digital removal of connective tissue components and skin allows the microcalcifications to be highlighted for the radiologist.

E. Breast Cyst Fluid Analysis

It is important to have high specificity in breast imaging to avoid unnecessary biopsies in women who have benign disease, particularly in those women with dense breast tissue. Full 3D inverse scattering ultrasound tomography has the advantage of high-fidelity and spatial

resolution and its ability to provide quantitative measurements. Thus, closely pack structures (such as cells in a suspension) exhibit higher effective refractive index, and higher cell counts within breast cysts result in higher value of refractive index, with a consequent increase in speed of sound within the cyst (27). A breast cyst demonstrating this is shown in **Figure 20**. The correlation of cell count with speed of sound in macro cysts is consistent with the presence of cell number observed cytologically as shown in **Figure 21**.

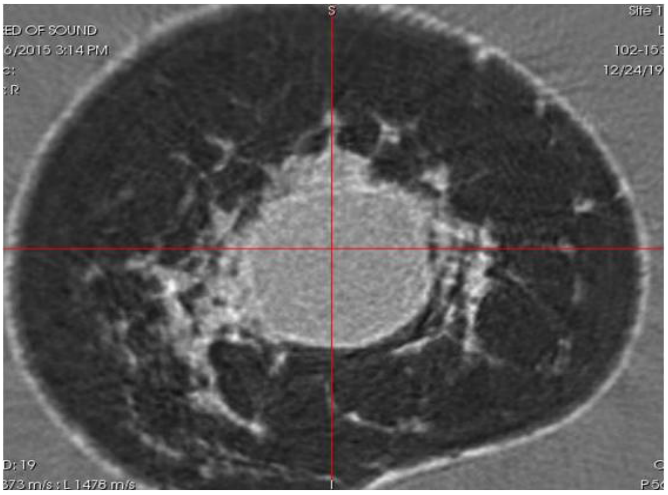

Figure 20: This figure demonstrates a breast microcyst containing relatively high speed "speckled" contents indicating clumps of cells within the cyst fluid.

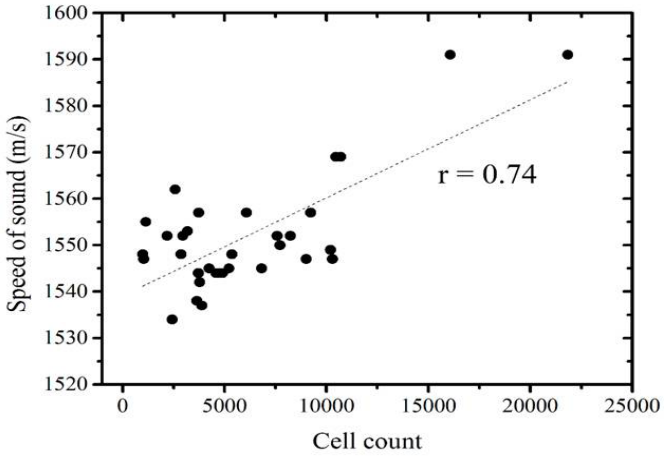

Figure 21: Graph showing the correlation between cyst fluid cell counts and sped of sound.

The importance of this finding is that no other mesoscopic imaging modality can capture such quantitative variation as a function of cell count. Based on our work with speed as a classifier, we can define a spectrum of breast macro cysts from fluid-filled to highly cellular with high speed cysts being mature macro cysts with high cell counts and many cellular clumps that correlate with cyst microanatomy as seen by transmission ultrasound. The clinical relevance of our work is that this technique will allow the breast imaging radiologists to have a basis for describing breast macro cysts and for following changes in these masses over time.

F. Chest Wall Imaging in Breast Cancer Screening

Imaging of the posterior portion of the breast is important because this region represents the posterior limit of active breast tissue. To be effective and comprehensive, breast screening methods must be able to evaluate this region. The use of full 3D inverse scattering has several advantages over 2D imaging technologies in visualization of the posterior breast. Under full 3D inverse scattering, image data is acquired in 3D, allowing for interpretation of data sets very far posteriorly in the breast. Inverse scattering reconstruction then permits use of data beyond the direct "line-of-sight" of conventional linear transducer signals, allowing for the analysis of the scattered signal data outside of the direct line-of-sight energy [17,18]. An illustration of the 2D line-of-sight reconstruction versus the full 3D inverse scattering reconstruction is shown in **Figures 22** and **23**.

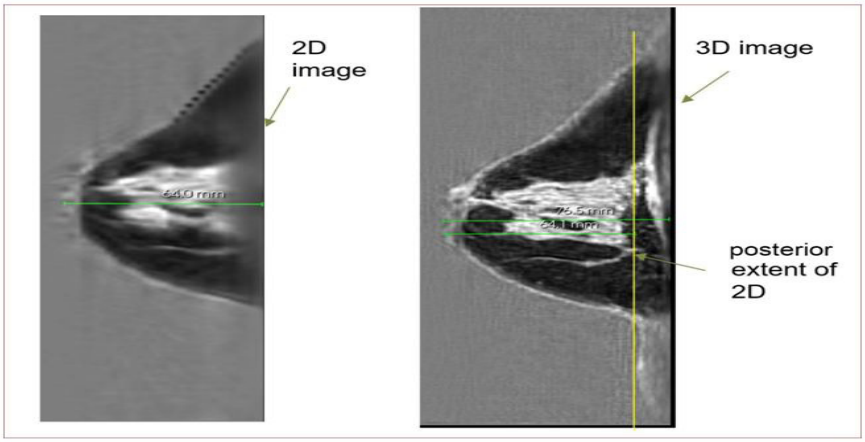

Figure 22: Comparison of 2D (left panel) vs full 3D reconstruction of a breast (right panel). The QT image exhibits higher resolution and cannot see the posterior limit of the glandular tissue or the pectoralis muscle (white crescent).

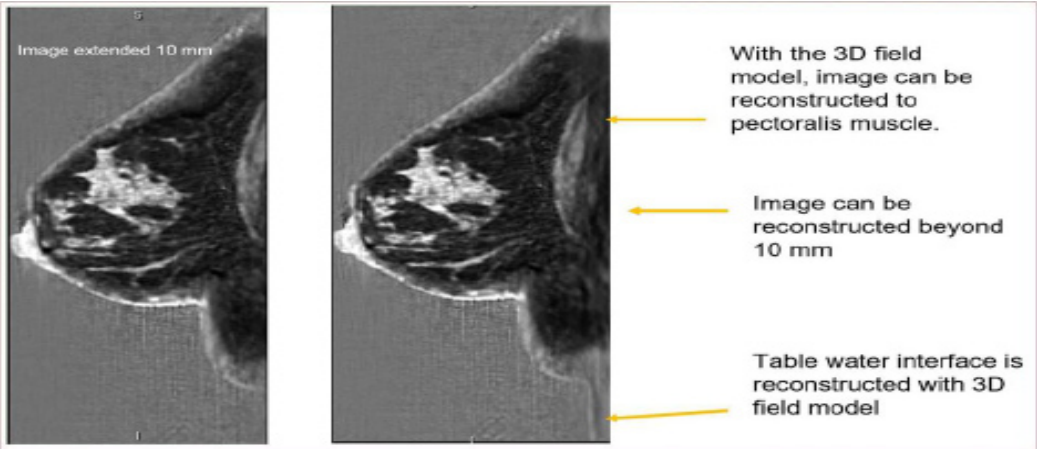

Figure 23: Full 3D reconstruction of a breast (left panel) with 10mm extension beyond the last acquisition level and a further extension of full 3D reconstruction (right panel) using the inverse scattering algorithm.

8. Conclusions

We conclude that full 3D inverse scattering ultrasound tomography is a novel method unused by others in medical imaging. The technology has a unique mechanical architecture capable of acquiring speed of sound and reflection images in 3D. The image reconstruction is computationally challenging and involves solving complex equations using high-performance computing. Laboratory studies demonstrate that the technique has high resolution and high contrast-to-noise ratios in both speed and reflection images. Clinical studies show that this technology is capable of visualizing breast microanatomy and breast microcalcifications along with providing a method for tissue classification using biomarkers. Finally, the technology has improved performance for imaging dense breasts. Full 3D inverse scattering ultrasound tomography offers unparalleled imaging of the breast including microanatomic features of the breast.

9. Acknowledgements

This work was supported in part by a grant from the U.S. National Cancer Institute (National Institutes of Health Grant R01 CA138536).

10. References

1. Woo Joseph. A short History of the Real-time ultrasound scanner. From: A short History of the developments of Ultrasound in Obstetrics and Gynecology; 1998; cited 2018 March 18. Available from: http://www.ob-ultrasound.net/history-realtime.html

2. Kaveh M, Mueller RK, Rylander R, Coulter TR, Soumekh M. Experimental Results in Ultrasonic Diffraction Tomography. In: Wang KY, editor. Acoustical Imaging: Visualization and Characterization. Boston, MA: Springer US, 1980; p. 433-450.

3. Radon J. Mengen konvexer Körper, die einen gemeinsamen Punkt enthalten. Mathematische Annalen.1921; 83:113-115.

4. Greenleaf JF, Johnson SA, Lee SL, Hermant GT, Woo EH. Algebraic Reconstruction of Spatial Distributions of Acoustic Absorption within Tissue from Their Two-Dimensional Acoustic Projections. In: Green PS, editor. Acoustical Holography: Volume 5. Boston, MA: Springer US, 1974; p. 591-603.

5. Greenleaf JF, Johnson SA, Lent AH. Measurement of spatial distribution of refractive index in tissues by ultrasonic computer assisted tomography. Ultrasound in Medicine & Biology1978; 3:327-339.

6. Johnson SA, Tracy ML. Inverse Scattering Solutions by a Sinc Basis, Multiple Source, Moment Method -- Part I: Theory. Ultrasonic Imaging 1983; 5:361-375.

7. Tracy ML, Johnson SA. Inverse scattering solutions by a sinc basis, multiple source, moment method - part II: Numerical evaluations. Ultrasonic Imaging 1983; 5:376-392.

8. Johnson SA, Zhou Y, Tracy MK, Berggren MJ, Stenger F. Inverse scattering solutions by a sinc basis, multiple source, moment method-Part III: Fast algorithms. Ultrasonic Imaging 1984; 6:103-116.

9. Andre M, Janee H, Otto G, Martin P, Spivey B, Palmer D. High speed data acquisition in a diffraction tomography system employing large-scale toroidal arrays. Int. J. Imaging Syst. Technol 1997; 3:137-147.

10. Carson PL, Meyer C, Scherzinger A, Oughton T. Breast imaging in coronal planes with simultanious pulse echo and transmission ultrasound. Science 1981; , pp. 1141-1143, 1981.

11. Li C,Duric N, LittrupP, Huang L. In Vivo Breast sound-speed imaging with ultrasound tomography. Ultrasound. Med. Biol.2009;35:1615-1628.

12. Fatemi M, Greenleaf JF. Vibro-acoustography: An imaging modality based on ultrasound-stimulated acoustic emission. Proc. Natl. Acad. Sci., U.S.A. 1999; 96:6603-6608.

13. Duric ND, Li C, Littrup P, et al. Detection and characterization of breast masses with ultrasound tomography: clinical results. Proceedings Volume 7265; Medical Imaging 2009; Ultrasonic Imaging and Signal Processing; 72651G; doi:10.1117/12.812994

14. Wiskin J, Borup D, Johnson S, Berggren M. Non-linear inverse scattering: High resolution quantitative breast tissue tomography.J. Acoust. Soc. Am. 2012; 131:3802;http://dx.doi.org/10.1121/1.3699240, (also in Vir. J. Bio. Phys. Res., Vol. 23, (10), Instrumentation and Development)

15. Glover GH. Computerized time-of-flight ultrasonic tomography for breast examination. Ultrasound in Medicine & Biology 1977; 3: 117-127.

16. Greenleaf JF, Bahn RC. Clinical imaging with transmissive ultrasonic computerized tomography. Biomedical Engineering, IEEE Transactions1981; 2:177-185.

17. Wiskin JW, Borup DT, Iuanow E, Klock J, Lenox MW. 3-D Nonlinear Acoustic Inverse Scattering: Algorithm and Quantitative Results; IEEE TRANSACTIONS ON ULTRASONICS, FERROELECTRICS, AND FREQUENCY

CONTROL 2017; 64:1161-1174.

18. Wiskin JW, Klock JC, Malik B, Natesan R, Lenox MW. Ultrasound Tomography of the Human Breast. International Symposium on Biologic Imaging 2018. Presented at Washington DC April 5, 2018, Abstract FrS2T1.5

19. Lenox MW, Wiskin JW, Lewis MA, Darrouzet S, Borup D, Hsieh S. Imaging Performance of Quantitative Transmission Ultrasound; International Journal of Biomedical Imaging 2015; Article ID 454028. doi:10.1155/2015/454028

20. Malik, B. , Terry, R. , Wiskin, J. and Lenox, M. (2018), Quantitative transmission ultrasound tomography: Imaging and performance characteristics. Med. Phys.. . doi:10.1002/mp.12957

21. Nickson C, Kavanagh A, Tumor size at detection according to different measures of mammographic breast density. J. Med. Screen 2009; 16:140-146.

22. Malik, B, Klock JC, Wiskin JWW, Lenox MW. Objective breast tissue image classification using Quantitative Transmission ultrasound tomography. Nature Sci. Rep.2016; 6:38857; doi: 10.1038/srep38857.

23. Klock JC, Iuanow E, Malik B, Obuchowski NA, Wiskin JW, Lenox MW. Anatomy-Correlated Breast Imaging and Visual Grading Analysis Using Quantitative Transmission Ultrasound. International Journal of Biomedical Imaging Volume 2016, Article ID 7570406, 9 pages

24. Iuanow E, MD, Smith K, Obuchowski NA, Bullen J, Klock JC. Accuracy of Cyst vs. Solid Diagnosis in the Breast Using Quantitative Transmission (QT) Ultrasound. Academic Radiology 2017; 24:1148-1153; doi: 10.1016/j.acra.2017.03.024. Epub 2017 May 23; PubMed ID 28549870.

25. Klock JC, Iuanow E, Smith K, Obuchowski NA. Visual Grading Assessment of Quantitative Transmission Ultrasound Compared to Digital X-ray Mammography and Hand-held Ultrasound in Identifying Ten Breast Anatomical Structures. BAOJ Clinical Trials 2017; 3:15.

26. Malik B, Terry A, Klock J, Lenox M. Sensitivity of Quantitative Transmission ultrasound to detection of micro calcifications. SPIE (International Society for Optics and Photonics) Meeting Houston Texas February 20, 2018.

27. Malik B, Klock JC. Breast Cyst Fluid Analysis Correlations with Speed of Sound Using Transmission Ultrasound. Academic Radiology 2018; (In Press).